Biochimica et Biophysica Acta 1818 (2012) 411–424

Contents lists available at SciVerse ScienceDirect

Biochimica et Biophysica Acta

journal homepage: www.elsevier.com/locate/bbamem

Elastic, electrostatic and electrokinetic forces influencing membrane curvature

M. Tajparast [a], M.I. Glavinović [b,*]

[a] Department of Civil Engineering and Applied Mechanics, McGill University, Montreal, PQ, Canada
[b] Department of Physiology, McGill University, Montreal, PQ, Canada

ARTICLE INFO

Article history:
Received 23 May 2011
Received in revised form 14 September 2011
Accepted 18 October 2011
Available online 26 October 2011

Keywords:
Lipid bilayer
Poisson–Nernst–Planck
Maxwell stress
Coulomb force
Dielectric force
Spontaneous curvature

ABSTRACT

Many cellular and intracellular processes critically depend on membrane shape, but the shape generating mechanisms are still to be fully understood. In this study we evaluate how electrostatic/electrokinetic forces contribute to membrane curvature. Membrane bilayer had finite thickness and was either elastically anisotropic or anisotropic overall, but isotropic per sections (heads and tails). The physics of the situation was evaluated using a coupled system of elastic and electrostatic/electrokinetic (Poisson–Nernst–Planck) equations. The fixed charges present only on the upper membrane surface lead to the accumulation of counterions and depletion of co-ions that decay spatially very rapidly (Debye length<1 nm), as does the potential and electric field. Spatially uneven electric field and the permittivity mismatch also induce charges at the membrane–solution interface, which are not fixed but influence the electrostatics nevertheless. Membrane bends due to — Coulomb force (caused by fixed membrane charges in the electric field) and the dielectric force (due to the non-uniform electric field and the permittivity mismatch between the membrane and the solution). Both act as membrane surface forces, and both depend supra-linearly on the fixed charge density. Regardless of sign of the fixed charges, the membrane bends toward the charged (upper) surface owing to the action of the Coulomb force, but this is opposed by the smaller dielectric force. The spontaneous membrane curvature becomes very pronounced at high fixed charge densities, leading to very small spontaneous radii (<50 nm). In conclusion the electrostatic/electrokinetic forces contribute significantly to the membrane curvature.

1. Introduction

Membranes are one of the most basic components of living cells and play a variety of roles. They separate cells and intracellular organelles from their surroundings, partition the space and delimit metabolic pathways thus providing the complex hierarchy of intracellular biochemical compartments. Membranes also control the transport mechanisms between various compartments. Finally, cellular membranes have areas of high curvature (this is often even more pronounced for the membranes of sub-cellular organelles), although the membranes resist bending, because bending typically (but not always) requires energy [1–3]. Bending may be energy cost-free, given the proper distribution of the lipids and/or proteins within the membrane. It is thus of considerable interest to understand what the shape-generating mechanisms are.

In a variety of biophysical and biochemical processes the shape of the membrane plays a variety of other, but critical roles [4]. It may promote a redistribution of proteins anchored in membranes through an action of hydrophobic moieties by introducing packing defects (greater free space) that become adsorption sites for amphiphilic molecules [5]. In some cases, such as exocytosis, endocytosis and vesiculation, the mechanical membrane properties are very directly linked to biological functions, and these processes are associated with pronounced membrane deformation [6–8]. The membrane curvature and its mechanical properties may also influence the action of a variety of membrane proteins and lipids [9–13,5].

Membrane shape can be regulated dynamically, and this occurs during a variety of cellular processes such as exocytosis and endocytosis [7,14,15], mitosis [16] or during protein transport from the endoplasmic reticulum to the Golgi body during secretion [17,18] and various physical mechanisms appear to be involved [19,7,20,4,8,21], but their relative importance and interplay are still to be worked out.

Considerable attention has been given to determining the mechanisms by which proteins generate mechanical forces to bend the membrane and establish the areas of high membrane curvature [22,23,7,24]. Although it has been suggested long ago that the Coulomb forces caused by the asymmetry of fixed charges on the membrane, or by the asymmetry of screening charges could also alter the membrane shape and induce membrane curvature [25–29], this mechanism received less attention. This is somewhat surprising since a variety of processes may lead to charge asymmetry. They include changes of pH or ionic strength in the solution, phosphorylation of inositol lipids [30], or cleavage of the acyl chains by phospholipases. Since changes of pH and ionic

* Corresponding author at: Department of Physiology, McGill University, 3655 Sir William Osler Promenade, Montreal, P.Q., Canada H3G 1Y6. Tel.: +1 514 398 6002; fax: +1 514 398 7452.
E-mail address: mladen.glavinovic@mcgill.ca (M.I. Glavinović).

0005-2736/$ – see front matter © 2011 Elsevier B.V. All rights reserved.
doi:10.1016/j.bbamem.2011.10.017

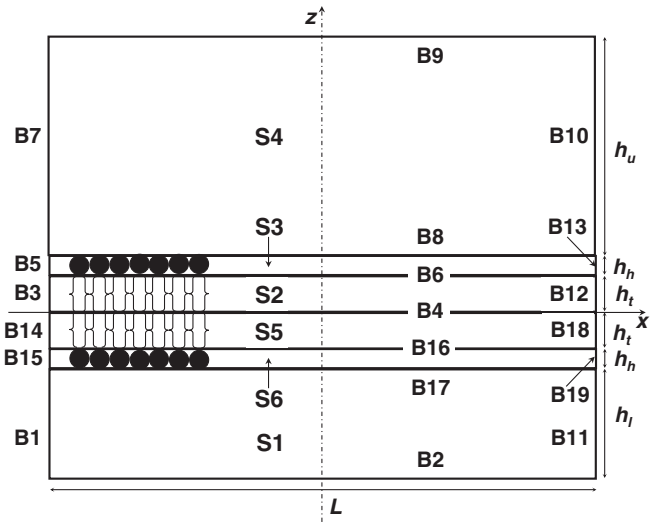

Fig. 1. Schematic representation of the lipid bilayer in the *x*-*z* plane. The membrane height h is divided into the hydrophilic heads (closed circles) with the height h_h and the hydrophobic tails (h_t) sections. L is the membrane length, and h_u and h_l are the heights of the upper and lower compartments with the electrolyte solution. The membrane plane is centered at the origin, and its thickness t_m is 100 nm. L is 20 nm, h is 2 nm, h_h is 0.7 nm, $h_u = 8$ nm, and $h_l = 4$ nm. S_i (i = 1–6) and B_j (j = 1–19) stand for the subdomains and boundaries of the lipid bilayer, respectively, and are defined in Table 1.

strength, phosphorylation of inositol lipids or cleavage of the acyl chains by phospholipases not only affect the charge density at the membrane surface, but also have other effects, it is not possible to separate them. The simulations are thus needed to evaluate the membrane bending due to electrostatic/electrokinetic forces.

The membrane may bend even if the membrane is not charged, but is present in a non-uniform electric field, given a permittivity mismatch between the membrane and the solutions that surround it (intra-cellular and extracellular), which is very pronounced. This force ('dielectric' force), which was first defined by Pohl [31] induces an asymmetric distribution of the electrical stress, that however can be determined from the Maxwell stress tensor [32–34]. Its contribution to membrane bending has been ignored hitherto. We determined the electrostatic/electrokinetic forces and the membrane deformation by evaluating a coupled system of linear elastic equations and electro-static–electro-kinetic (Poisson–Nernst–Planck) equations. The ionic concentrations and composition were as observed physiologically, and the density of fixed charges ranged from 0 mC/m^2 to 128 mC/m^2. Note that if the mean area of a lipid molecule is assumed to be 0.5 nm^2, 40% of lipid molecules would have to have 1 electron charge at the highest density of fixed charges (i.e. 128 mC/m^2). The 'membrane potential' (i.e. the potential difference between the intra-cellular and extra-cellular compartments) was either 0 or −80 mV. The simulations demonstrate that the Coulomb force can significantly contribute to the spontaneous curvature, and that the largely ignored dielectric force curtails its action, but only to a limited extent.

2. Methods

2.1. Geometry

We evaluate the deformation of a segment of membrane lipid bilayer caused by the electrostatic forces generated by the presence of fixed charges on the internal side of the bilayer, or by the potential difference between two compartments bathing the bilayer. The intracellular (i.e. upper) compartment contained an electrolyte solution made of K^+ and Cl^-, whereas the extracellular (or lower) compartment contained Na^+ and Cl^-. The flat lipid membrane is considered as a two-dimensional (2D) sheet in the *x*-*y* plane of the Cartesian coordinate system (x, y, z) with the center of the lipid bilayer in the origin. Fig. 1 depicts the schematic representation of the lipid bilayer. To account for the amphiphilic nature of each lipid monolayer, we divide it into two regions — one with hydrophilic heads and another with hydrophobic tails. The height of the lipid monolayer h is 2 nm, its head section h_h is 0.7 nm, whereas the tail section h_t is 1.3 nm. The length of the membrane $L = 20$ nm and its thickness t_m is 100 nm, h_u (= 8 nm) and h_l (= 4 nm) denote the heights of the upper and lower compartment respectively. The subdomains and boundaries of the lipid bilayer are S_i and B_j respectively, where i = 1–6 and j = 1–19.

To analyze the structural deformation of the lipid membrane we consider the plane-stress model in the associated subdomains (i.e., 2, 3, 5, and 6). Furthermore, the Poisson equation describing the electrostatics is defined in all the subdomains. The Nernst–Planck equation describes the electrokinetic flow and accounts for the movement (i.e., diffusion and migration) of ions in the electrolyte media and is active in subdomains 1 and 4. The membrane is assumed to be impermeable to movement of ions. Table 1 gives all boundary conditions and Table 2 details all parameters and constants.

2.2. Calculating the Coulomb and dielectric forces — Maxwell stress tensor

In a given subdomain, the Maxwell stress tensor (**S**) is expressed as follows:

$$\mathbf{S} = e_r e_0 \left[\mathbf{EE} - \frac{1}{2}(\mathbf{E}.\mathbf{E})\mathbf{I} \right] \tag{1}$$

where e_r is the relative permittivity in the subdomain and e_0 is the permittivity of vacuum, **E** is the electric filed vector $(E_x, E_z)^T$, and **I** is the identity tensor [33,35]. We compute the Maxwell stresses in the membrane and in two compartments containing the liquid electrolyte. The contribution of the dielectric force due to the Maxwell stress

Table 1
Boundary conditions.

Boundary	Plane stress	Electrostatics	Electro-kinetics
B1, B7, B10, B11	NA	Zero charge symmetry	Insulation symmetry
B2	NA	Electric potential V_d	Concentration C_{i0d}
B3, B5, B12, B13, B14, B15, B18, B19	*x*-*y* symmetry plane	Zero charge symmetry	NA
B4, B6, B16	Continuity	Continuity	NA
B8	Prescribed displacement: u and w in x and z directions, respectively; Applied total force due to Maxwell stress tensor and charged surface (F_{e8})	Surface charge density σ_{e8}	Insulation symmetry
B9	NA	Electric potential V_u	Concentration C_{i0u}
B17	Prescribed displacement: u and w in x and z directions, respectively; Applied force due to Maxwell stress tensor (F_{e17})	Surface charge density σ_{e17}	Insulation symmetry

Table 2
Model parameters and constants.

Params	Value	Description	Unit	Refs
$\mathbf{C_{10u}}$	150.0	K^+ concentration (upper compartment)	mol/m^3 or mM	
$\mathbf{C_{20u}}$	150.0	Cl^- concentration (upper compartment)	mol/m^3 or mM	
$\mathbf{C_{30u}}$	0	Na^+ concentration (upper compartment)	mol/m^3 or mM	
$\mathbf{C_{10d}}$	0	K^+ concentration (lower compartment)	mol/m^3 or mM	
$\mathbf{C_{20d}}$	150.0	Cl^- concentration (lower compartment)	mol/m^3 or mM	
$\mathbf{C_{30d}}$	150.0	Na^+ concentration (lower compartment)	mol/m^3 or mM	
$\mathbf{D_1}$	1.960×10^{-9}	Diffusion coefficient of K^+ ions	m^2/s	[8,37]
$\mathbf{D_2}$	2.030×10^{-9}	Diffusion coefficient of Cl^- ions	m^2/s	[8,37]
$\mathbf{D_3}$	1.330×10^{-9}	Diffusion coefficient of Na^+ ions	m^2/s	[8,37]
e	1.602×10^{-19}	Elementary charge	C	
R	8.314	Universal gas constant	J/(mol.K)	
T	300.0	Temperature	K	
$\mathbf{V_u}$	-8.000×10^{-2}	Electric potential (controlling edge of the upper compartment)	V	
$\mathbf{V_d}$	0	Electric potential (controlling edge of the lower compartment)	V	
$\boldsymbol{e_0}$	8.854×10^{-12}	Permittivity of vacuum	F/m	
$\boldsymbol{e_{rw}}$	80.0	Relative permittivity of the electrolyte media	Dimensionless	[33,42]
$\boldsymbol{e_{rm}}$	2.0 (or 8.0)	Relative permittivity of the membrane	Dimensionless	[8]
$\boldsymbol{\rho_m}$	785.0	Membrane density	kg/m^3	[8]
$\boldsymbol{\sigma_{e8}}$	-8.000×10^{-3} or as specified	Surface charge density of the upper boundary of the membrane bilayer (B8)	C/m^2	[36,37]
$\boldsymbol{\sigma_{e17}}$	0	Surface charge density of the lower boundary of the membrane bilayer (B17)	C/m^2	
$\boldsymbol{\nu}$	0.330	Poisson's ratio	Dimensionless	
$\boldsymbol{\lambda_{mhxxxx}}$	4.000×10^9	Young's modulus of volume stretching-compression in lateral direction (heads)	Pa	[4]
$\boldsymbol{\lambda_{mhxxzz}}$	3.930×10^9	Young's modulus of coupling between lateral and normal deformation (heads)	Pa	[4]
$\boldsymbol{\lambda_{mhzzzz}}$	4.000×10^9	Young's modulus of volume stretching-compression in normal direction (heads)	Pa	[4]
$\boldsymbol{\lambda_{mtxxxx}}$	1.000×10^9	Young's modulus of volume stretching-compression in lateral direction (tails)	Pa	[4]
$\boldsymbol{\lambda_{mtxxzz}}$	0.980×10^9	Young's modulus of coupling between lateral and normal deformation (tails)	Pa	[4]
$\boldsymbol{\lambda_{mtzzzz}}$	1.000×10^9	Young's modulus of volume stretching-compression in normal direction (tails)	Pa	[4]

tensor $\mathbf{F_M} = (F_{Mx}, F_{Mz})^T$ to the total force acting on the boundaries B8 and B17 is thus:

$$\mathbf{F_M} = \int_\Omega \mathbf{n}.\mathbf{S}dA = t_m \int_{\partial\Omega} \mathbf{n}.\mathbf{S}dl \quad (2)$$

where Ω represents one of the horizontal surfaces of the membrane with the B8 or B17 edges, and which extend in the y-axis direction with the thickness t_m. **n** is the outward unit vector normal to each surface, and dA is the differential surface area element. $\partial\Omega$ is the membrane boundary (i.e., B8 or B17); dl is the differential boundary element.

In addition to the forces due to the Maxwell stresses from the lipid membrane and from the electrolyte media, there is a Coulomb force, or force due to the charges on the membrane surface in the electric field, which is:

$$\mathbf{F}_\sigma = t_m \sigma_e \mathbf{E} \quad (3)$$

where σ_e is the surface charge density at the boundaries B8 or B17. σ_e ranges from 4 mC/m^2 to 128 mC/m^2. These values are comparable or below values estimated for the cell membrane (one elementary negative fixed charge per 1–4 nm^2, which corresponds to a charge density of 40–160 mC/m^2; [36,37]. Finally, σ_{e17} is zero. The total force $\mathbf{F_e}$ that drives the membrane deformation is the sum of the $\mathbf{F_M}$ and $\mathbf{F_\sigma}$ forces acting on the boundaries B8 or B17; that is, F_{e8} or F_{e17}, respectively.

The system of coupled equations given by the Poisson–Nernst–Planck and elastic equations (see Appendix A) was solved by finite element method using a commercial software package program Comsol 3.5 (Comsol, Burlington, MA, USA), whereas the postprocessing was performed using a software package for scientific and engineering computation Matlab (MathWorks, Natick, MA, USA).

3. Results

3.1. Spatial distribution of ions, potential and electric field

Fig. 2A–B depicts the spatial distribution of ions (K^+ and Cl^- in the upper (intracellular) compartment, and Na^+ and Cl^- in the lower (extracellular) compartment, in the absence (A) and in the presence (B) of the 'resting potential' (i.e. potential difference between two compartments). Fig. 2C–D shows the spatial distribution of potential in the absence (C) and in the presence (D) of the 'resting potential'. Finally, Fig. 2E–F shows the spatial distribution of electric field in the absence (E) and in the presence (F) of the 'resting potential'. Note that the 'resting potential' is determined at two controlling edges at the top and the bottom of the simulation space (see Methods section). In the presence of fixed charges the charge accumulations are quite large, and as a result the potential profiles and electric field profiles (z-component) within the membrane and in the solution are affected significantly. Very rapid spatial decay of charges in the solution is also associated with similarly rapid decay of the potential and the electric field in the solution above the membrane surface with the fixed charges. Finally, the potential and the electrical field profiles in the membrane (though much less so in the solution) are also affected by the 'resting potential'.

3.2. Dependence of the surface potential and the electric field on fixed charge density and 'resting potential'

Both the Coulomb force and the dielectric force acting on the membrane can be calculated if the permittivity of the membrane and of the solution, the electric field on the membrane surface and the fixed charge density are known. It is not necessary to know what the values of the electric field are either within the membrane or in the solution (see Methods section). Since the electric field and the potential are spatially highly not uniform near the membrane surface owing to the presence of fixed charges, we show in a separate figure how both the electric field and the potential depend on the density of the fixed charges at the upper membrane surface, and how they are modulated by the 'resting potential'.

The potential at the upper surface of the membrane depends approximately linearly on both the density of the fixed charges at the upper membrane surface (regardless of the sign of fixed charges; Fig. 3A), and on the 'resting potential' (Fig. 3B). The dependence of the electric field (z-component) at the upper surface of the membrane on the density of the fixed charges (Fig. 3C), and on the 'resting potential' (Fig. 3D) is also approximately linear. In addition to the electric field at the upper membrane surface (filled symbols) we also show the electric field in the middle of the membrane (empty

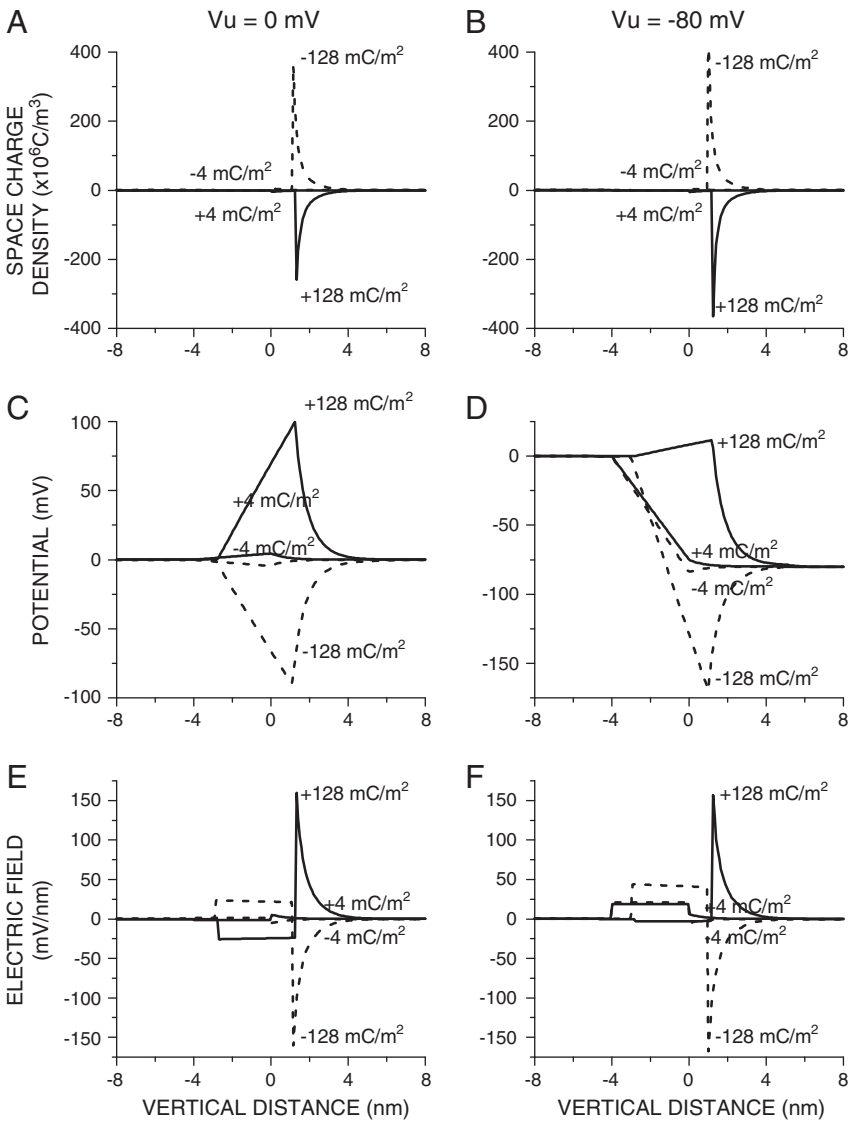

Fig. 2. Presence of the fixed charges on the membrane surface leads to great accumulations of charges in the solution (A–B), and such accumulations significantly alter the potential profiles (C–D) and electrical field profiles (its *z*-component; E–F) across the membrane and in the solution. Note a very rapid spatial decay of the space charge density, the potential and the electric field in the solution above the membrane surface with the fixed charges. As expected the potential and electrical field profiles are also affected by the 'resting potential' (potential difference between the controlling edges of two compartments on both sides of the membrane). All plots are the cross-sectional plots at $x = 0$ and with z varying from -8 nm to $+8$ nm.

symbols). Although they all show similar linear dependence on the 'resting potential', the values of the electric field in the middle of the membrane are very different from those at the upper membrane surface, although that is visually not easily discernible from their spatial distributions (Fig. 2E–F). In these simulations the permittivity of the membrane is taken to be 2 for the whole membrane (i.e. for both the head and tail sections). However, a higher value may also be considered for the head sections, given the highly polar nature of the headgroup region. As Fig. 3A shows the potential at the upper membrane surface differs very little if the permittivity of the head sections is 8 instead of 2. The magnitude of the z-component of the electric field differs more if the permittivity of the head sections is 8 instead of 2, but the difference remains marginal (Fig. 3C).

3.3. Spatial profiles of the displacement and polarization charge density and the electric field

Fig. 4 gives the cross-sectional plot of the displacement charge density (A), the polarization charge density (B), the displacement charge density in vacuum (C), the electric field (D), and the polarization space charge density (E). As expected the displacement charge density is much greater than it would have been in vacuum, and the reason is the polarization charge density. Note also that the polarization charge is almost entirely confined to the upper membrane surface. Fig. 4F compares how the fixed charge on the upper membrane compares with the polarization charges at the upper and lower membrane surfaces. The polarization charge on the lower solution–membrane interface is very small. The polarization charge on the upper solution–membrane interface, though smaller than the fixed charge, is not negligible. As expected the sign of the polarization charge on the upper surface is opposite of that of the fixed charge on the same surface. Finally, the absolute values of both the polarization charge and the fixed charge increase linearly as the density of fixed charges rises.

3.4. Coulomb and dielectric forces

Two forces are involved in bending the membrane — Coulomb force and dielectric force (see Methods section). Fig. 5C–E depicts

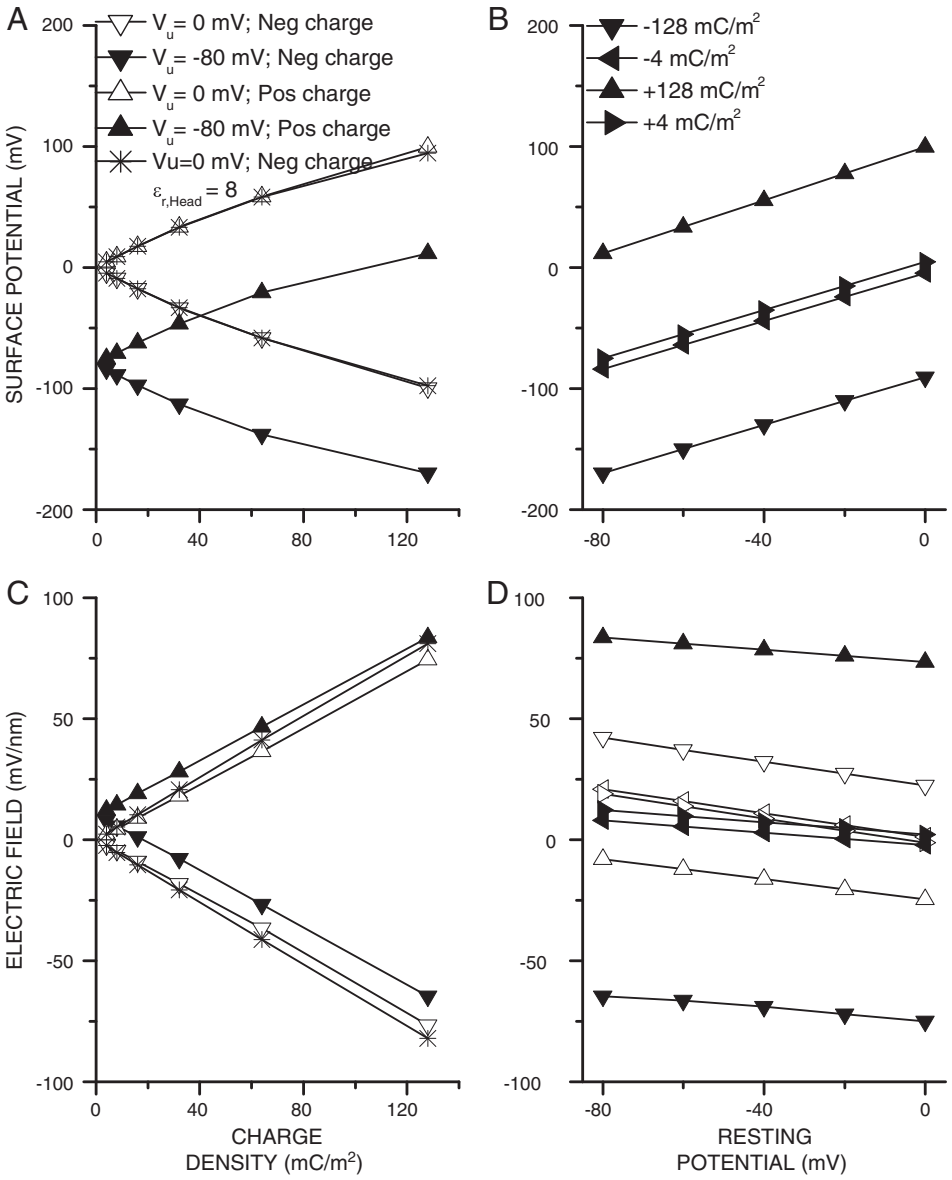

Fig. 3. A and B) Potential at the upper surface of the membrane depends on the density of the fixed charges at the upper membrane surface, and the relationship is approximately linear regardless of the sign of fixed charges. It also linearly depends on the 'resting potential'. C and D) The electric field (*z*-component) at the upper surface of the membrane is very strongly influenced by the density of the fixed charges, whereas its dependence on the 'resting potential' is less strong. Both relationships are linear regardless of the sign of the charges on the membrane surface. Note that the values of the electric field at the upper membrane surface (filled symbols) differ very significantly from those in the middle of the membrane (empty symbols), although their dependence on the 'resting potential' is very similar (D). If the permittivity of the head sections is higher (8 instead of 2; see text) both the potential at the upper membrane surface (A), and the magnitude of the z-component of the electric field (C) change only marginally.

how the dielectric force on the lower (external) and upper (internal) membrane surface changes as the charge density on the upper membrane surface increases. The dielectric force on the lower membrane surface (without the fixed charges), which is positive (i.e. it points upwards) is very small. The dielectric force on the upper membrane surface (with fixed charges), which is negative (i.e. it points downwards) becomes progressively greater as the density of fixed charges rises, and the relationship is supra-linear. The dielectric forces on either the upper or the lower membrane surface act always from the solution (higher permittivity) toward the membrane (lower permittivity), but given the difference in the electric field at two surfaces the dielectric force at the upper surface, which is much greater, prevails. The Coulomb force is positive (i.e. it points upwards), and also increases supra-linearly as the density of fixed charges increases. Neither the Coulomb force nor the dielectric force acting on the upper membrane surface is altered by the change of sign of fixed charges. The dielectric force opposes the Coulomb force, and curtails its action, but the total force on the membrane is dominated by the Coulomb force and acts from the membrane toward the surface with the fixed charges (i.e. upwards; Fig. 5F–H). Finally, note that the 'resting potential' influences both the dielectric force (Fig. 5D–E), and to a lesser extent the Coulomb force (Fig. 5G–H). Finally, two cartoons of the membranes deformed owing to the presence of low (-16 mC/m^2; Fig. 5A) and high (-128 mC/m^2; Fig. 5B) charge densities are also shown. The Coulomb force (acting upwards) and dielectric forces (acting downwards) are depicted by scaled arrows.

3.5. Membrane deformation

The membrane deformation is determined by the force applied. Given that the combined Coulomb and dielectric force rises as the fixed charge density of the membrane surface increases, the

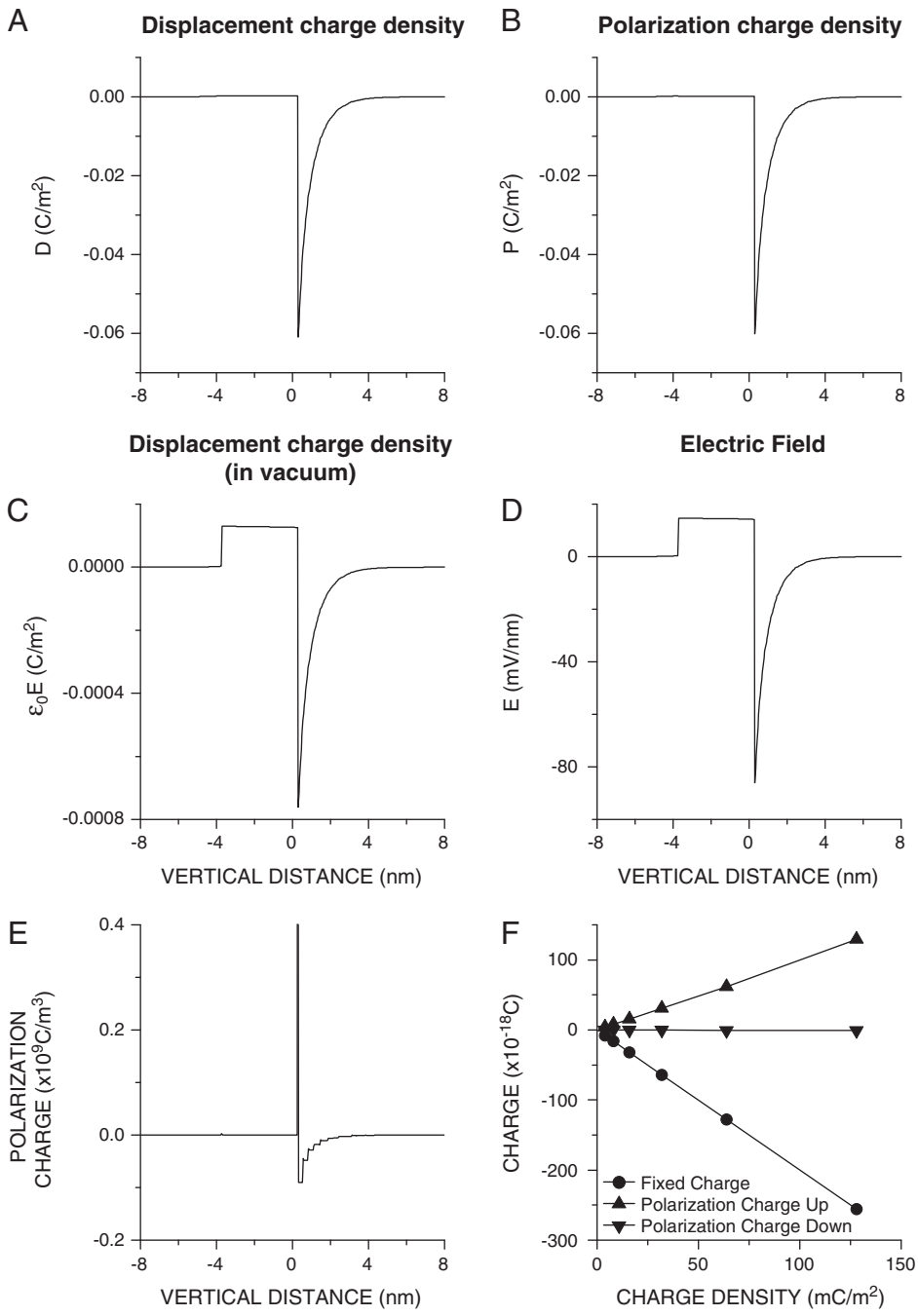

Fig. 4. Displacement charge density (A), polarization charge density (B) profiles and the profile of the displacement charge density in vacuum (C). Electric field profile (D). Polarization charge profile (E). Polarization charge on the upper surface of the membrane is smaller than the fixed charge on the same surface, though not negligible, and is opposite in sign, whereas the polarization charge on the lower membrane is very small (F). Polarization charge on the upper surface increases linearly with the fixed charge density on the same surface. All plots are the cross-sectional plots at $x=0$ and with z varying from -8 nm to $+8$ nm.

membrane deformation should and does reveal similar dependence. Fig. 6A–B gives the membrane displacement (i.e. the displacement of one point in the middle of the membrane) in z direction, when the density of fixed charges is low (4 mC/m^2; A) and high (128 mC/m^2; B). Fig. 6C shows the relationship between the density of fixed charges and membrane displacement. The displacement increases steeply and supra-linearly as density of fixed charges rises, but the sign of the charges affects the displacement very little. The 'resting potential' alters this relationship, but only marginally. If the displacement of the membrane is represented as an arc of the circle it is possible to calculate the radius of the circle ('spontaneous' radius R_s) from the length of the membrane l_m (20 nm) and the displacement di using the following formula $R_s=(4\times di^2+l_m^2)/(8\times di)$. Note that this is the 'spontaneous' radius of the tube (not sphere) since these simulations are two- and not three-dimensional. Fig. 6D gives the relationship between the fixed charge density and the 'spontaneous' radius R. Note that the relationship is shown on the semi-log scale. The 'spontaneous' radius at high density of fixed charges (>100 mC/m^2) is <50 nm. The spontaneous radius vs. charge density relationship remains qualitatively the same if longer membrane segments are simulated, but the spontaneous radii are smaller, and more so the longer the membrane segment is. Fig. 6E gives the relationship between the fixed charge density and spontaneous curvature (defined as 1/R). The spontaneous curvature

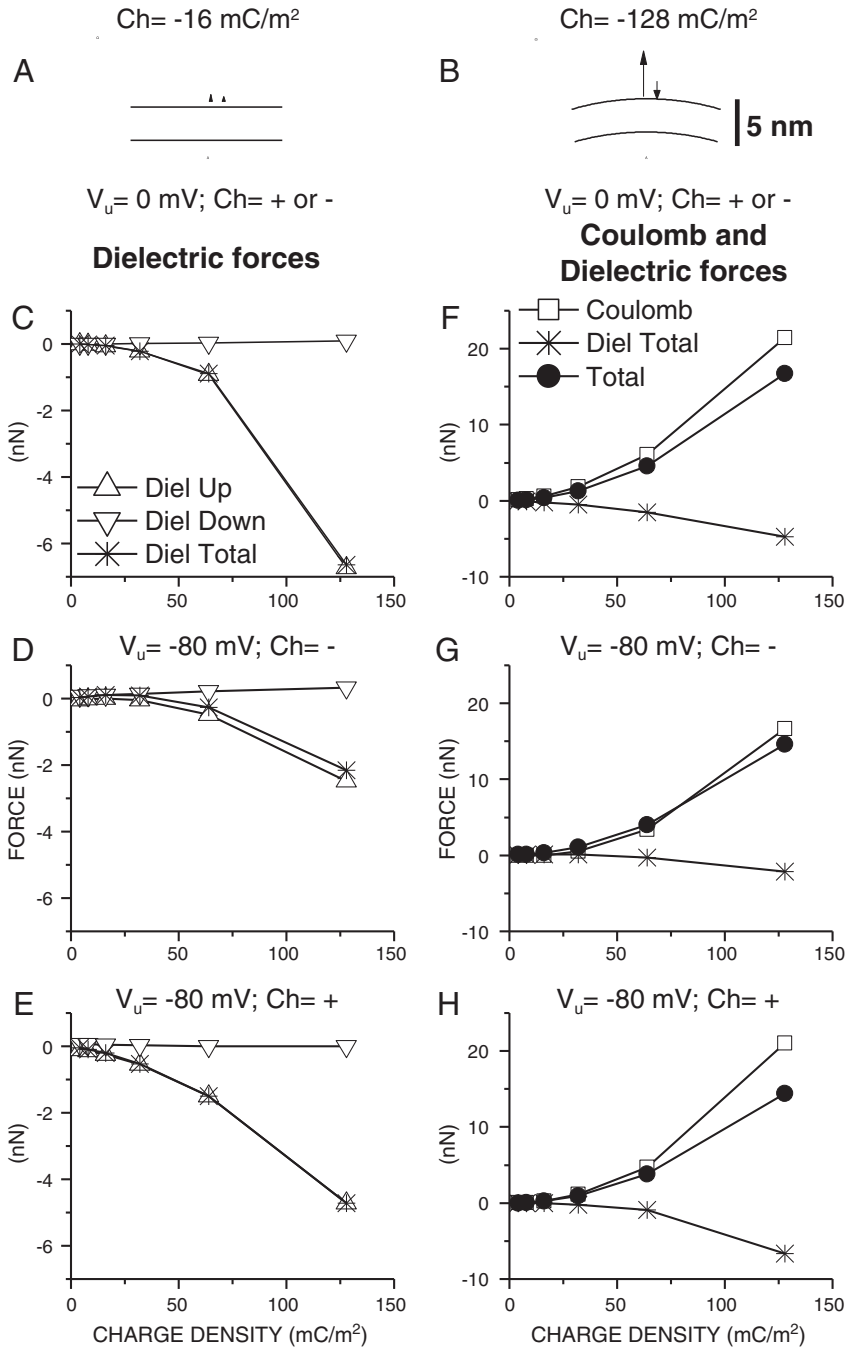

Fig. 5. Both the dielectric and the Coulomb forces are prominent on the internal (upper) membrane surface with fixed charges, and both become greater supra-linearly with the charge density. A–B) Sketches depict the extent of the membrane deformation (to scale) caused by the presence of the fixed charges on the upper membrane surface together with the scaled Coulomb and dielectric force arrows. The dielectric force (C–E) opposes the Coulomb force (F–H) and curtails its effect, but only to a limited extent. The potential difference between two compartments (upper and lower) also affects dielectric force (C–E), and to a lesser extent the Coulomb force (F–H). Neither the Coulomb force nor the dielectric force acting on the upper membrane surface is altered by the change of sign of fixed charges. The Coulomb force acting on the upper membrane surface (i.e. on the surface with the fixed charges) is always in that direction (i.e. in the direction of the surface with the fixed charges). In contrast, the dielectric forces on either the upper or lower membrane surface is from the solution (higher permittivity) toward the membrane (lower permittivity), but given the difference in the Coulomb field at two surfaces the dielectric force at the upper surface prevails. Combined dielectric force opposes the Coulomb force, and typically curtails its action. Nevertheless, the total force is typically dominated by the Coulomb force and acts in the direction of the surface with the fixed charges.

increases steeply with the density of fixed charges, and the steepness rises when simulated membrane segments are longer (E). Finally, the total peak displacement, the spontaneous radius and the spontaneous curvature remain almost identical, if the permittivity of the head sections is higher (8 instead of 2; not shown as they appear completely overlapping). This is not surprising given that the magnitude of the electric field (*z*-component) at the upper membrane surface is only marginally different when permittivity of the head sections is 8 instead of 2 (Fig. 3C).

3.6. True versus overall anisotropy

We also established the relationship between the fixed charge density and spontaneous radius, but assuming that the membrane is truly anisotropic instead of being anisotropic overall (i.e. with different, but individually isotropic elastic properties of the head and tail sections). There was no difference between two estimates of the charge density vs. spontaneous radius relationship, one simulated as a truly anisotropic case and another anisotropic overall.

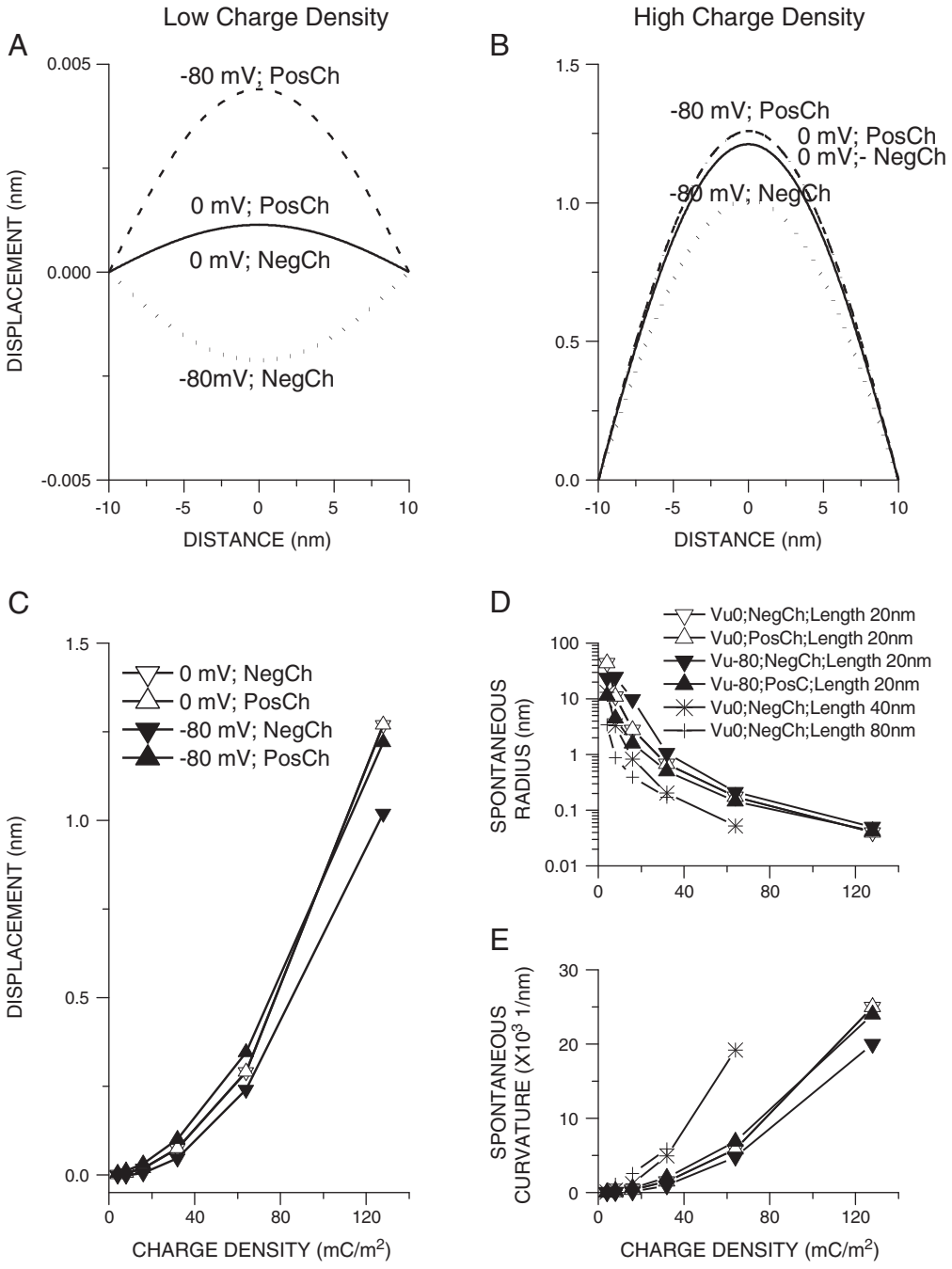

Fig. 6. Membrane deformation increases steeply as the density of fixed charges rises, but is also modulated, though modestly by the membrane potential. Membrane displacement at low (A) and high (B) charge densities. Note that the effect of the membrane potential (i.e. the potential difference between the upper and lower compartments) is relatively greater if the charge density is low. Peak displacement (displacement of the membrane at equal distance from two side edges) vs. charge density (C). The relationship is clearly supra-linear. The spontaneous radius is much lower at high density of fixed charges. This relationship remains qualitatively the same if longer membrane segments are simulated, but the spontaneous radii are lower, and more so the larger the membrane segment is (D; note a semi-log scale). The spontaneous curvature increases steeply with the density of fixed charges, and more so for larger membrane segments simulated (E). Finally, the peak displacement (C) and the spontaneous curvature (E) are only marginally greater, and the spontaneous radius only marginally smaller, if the head sections have four times higher permittivity (i.e. 8 instead of 2; D; not shown).

3.7. Maxwell stress force versus electrostatic pressure

The dielectric force (Maxwell stress force) acting on the elastic dielectrics that are planar before deformation is often approximated by the electrostatic pressure [38,35]. This amounts to representing the Maxwell stress tensor by a scalar (i.e. it amounts to representing $\mathbf{S} = e_r e_0 \left[\mathbf{EE} - \frac{1}{2}(\mathbf{E}.\mathbf{E})\mathbf{I}\right]$ with $S = (1/2)\cdot e_r e_0 E_z^2$), and whenever possible it is highly desirable, because it greatly simplifies simulations. This approach is justified whenever the tangential component of the electric field at the surface of the planar dielectric can be considered very small compared to the component of the electric field that is perpendicular to the planar dielectric. Since our simulations are of this kind, we compared the relationship between the fixed charge density and the spontaneous curvature, one obtained using a Maxwell stress and

another the electrostatic pressure to calculate the dielectric forces at two surfaces of the membrane (upper and lower). We find no difference between two estimates of the charge density vs. spontaneous radius relationship. The dielectric force can thus simply be calculated using the electrostatic pressure approach.

3.8. Dynamics of membrane deformation and elastic energy vs. displacement relationship

All simulations so far are steady-state simulations. Fig. 7A now gives how the electric force (i.e. the sum of the Coulomb and dielectric forces) and elastic force acting on the upper membrane surface change in time. Following an electrostatic, electrokinetic and elastic equilibration, the fixed charge (negative) density on the upper membrane surface was changed in a step-like manner from zero to 64 mC/m^2. Whereas the electric force remains constant following the change of charge density, the elastic force rises mono-exponentially with a time constant of ~1 ms until it matches the electric force. The membrane displacement follows the same time course (Fig. 7B). In contrast, the relationship between the elastic energy of the membrane and the membrane displacement is quadratic (Fig. 7C). Given the square relationship between the displacement and elastic energy it is not surprising that the elastic energy (of head and tail sections, but also total) does not change mono-exponentially with time, but is more sigmoidal (Fig. 7D).

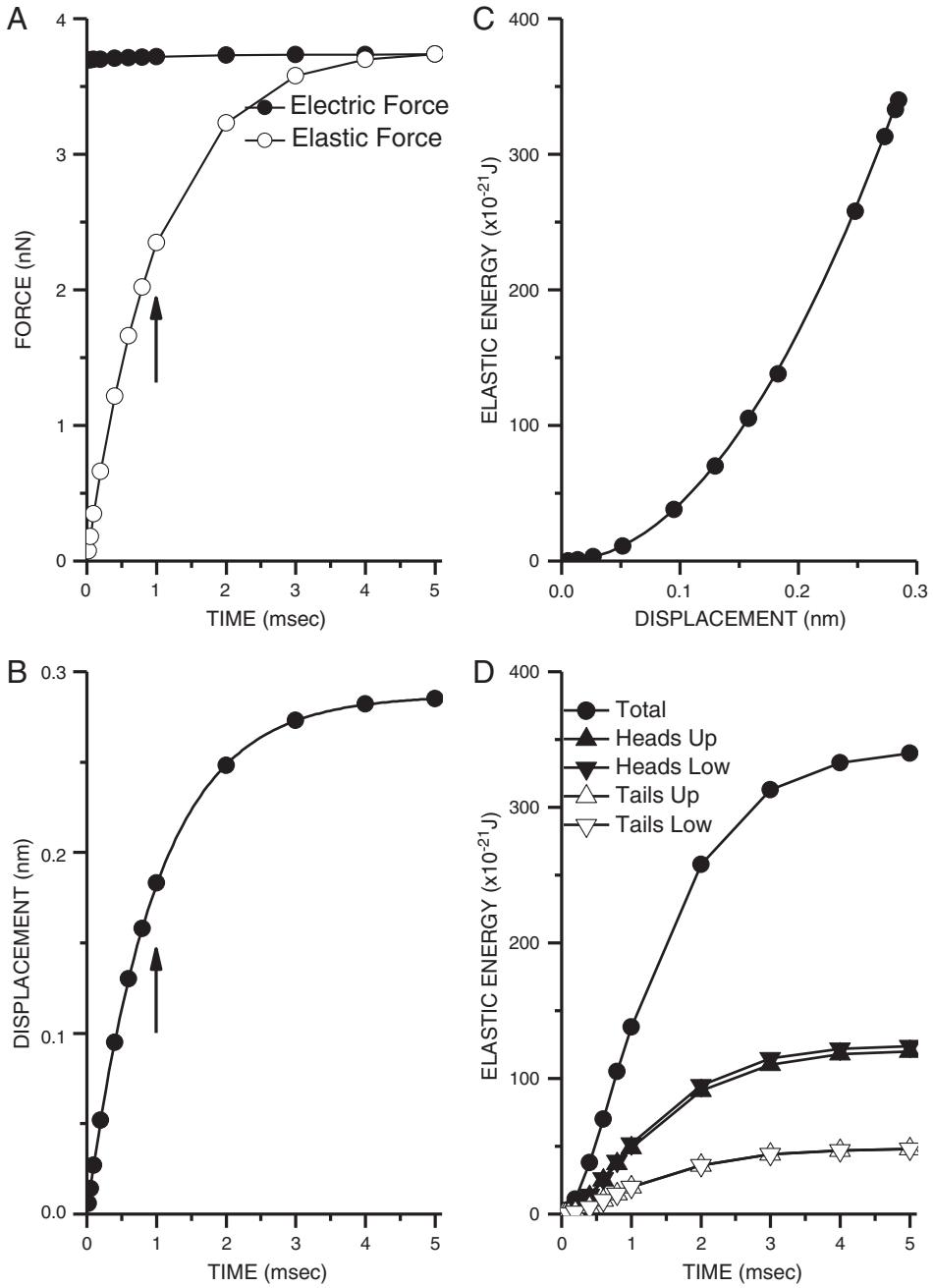

Fig. 7. Following a step-like change of charge density (from 0 to 64 mC/m^2 on the upper membrane surface, the electric force remains constant whereas the elastic force rises mono-exponentially with a time constant of ~1 ms, until it matches the electric force (A). The membrane displacement has the same time course (B). The elastic energy (EE) of the membrane vs. membrane displacement (di) relationship was fit by a second order polynomial, which was EE = 4225.6 × di^2, where EE is in 10^{-21} J and di is in nm (C). Time dependent change of the elastic energy of head and tail section and their sum is sigmoidal (D).

4. Discussion

4.1. Electrostatics and electrokinetics of the charged lipid bilayer in liquid electrolyte

The electrostatic/electrokinetic factors that contribute to bending of the membrane were evaluated using a coupled system of linear elastic equations [39,40] and electrostatic-electrokinetic (Poisson–Nernst–Planck) equations [41,42]. The membrane was assumed to be an elastic dielectric placed in a liquid electrolyte. The concentrations and composition of intra-cellular and extra-cellular solutions were as observed physiologically. The electrostatic variables (space charge density, potential, electric field, Maxwell stress tensor and Coulomb and dielectric forces), electrokinetic variables (ion concentrations) and elastic variables (membrane deformation, stress, traction, and elastic energy) were computed. The membrane bilayer was considered as an anisotropic elastic material overall, but the head and tail sections of the individual monolayers were isotropic, though possessing different elastic properties. Given that the head and tail sections of the membrane bilayer are anisotropic [4] we tested how a simplifying assumption that the sections are individually isotropic affects the results, but the effects were negligible. This is not surprising given very low level of anisotropy of either head or tail sections taken individually.

The electrostatics (the electric field and the potential) at any point in the simulation space are influenced by the density of fixed charges on the upper membrane surface. The presence of fixed charges leads to the accumulation of counter-ions and depletion of co-ions. The spatial decay of counter-ions and rise of co-ions is very rapid (and occurs in <2 nm), and is associated with a similarly rapid decay of the potential and the electric field. The potential and the electric field (its vertical or z component) on the intracellular membrane surface both depend on the 'resting potential (i.e. the potential difference between the intracellular and extracellular compartments, and on the fixed charge density, and in all cases the relationship is linear or nearly linear. Note however that this analysis describes the electrostatics and the electro-kinetics of the problem, but does not account for hydrodynamic effects, although the membrane is in solution on both sides. This will be part of a separate study.

4.2. Fixed and polarization charges

Dielectrics (and both membrane and water are dielectrics) are materials composed of electrically neutral small dipoles possessing internal charge separation [31,41]. If an external electric field is applied across a combination of dielectrics, such as a membrane in water, they become polarized, because single dipoles (permanent but also those induced by the electric field) in the dielectric medium tend to align themselves in the direction of the electric field. The positive end of individual dipoles will point toward lower potential, and the negative end toward the higher potential. As a result of such a rearrangement of dipoles net unpaired surface charges will accumulate at the membrane–water interface given that their dielectric properties are different [31]. These surface charges, which are generally not fixed, generate another electric field that adds to and distorts the original electric field. The amount of net unpaired charges at the membrane–water interface depends on the magnitude of the electric field, but also on the difference of dielectric properties of the membrane and the water, i.e. on the permittivity mismatch. The permittivity, which is a measure of the ability of dipoles within dielectric to reorient in an electric field, is very different for membrane and water, and is in this study taken to be 2 and 80 respectively. Finally, if the material is an electrolyte, the electric field will also give rise to charge movement (i.e. ion movement), which we evaluated using Nernst–Planck equations. We estimated the polarization charge on both the upper and the lower surfaces of the membrane. Given that this charge exists only in presence of an uneven electric field, the polarization charge should rise if the fixed charge density on the upper membrane surface increases, since that is the main mechanism generating the electric field, and it does. The polarization charge on the lower membrane surface is essentially zero, since the electric field at the lower surface is generally very low, but at the upper surface it is not negligible compared to the fixed charge.

4.3. Coulomb and dielectric forces

The study of electromechanical coupling (i.e. of mechanical forces generated by the electric field) in dielectrics that are also elastic materials is now a rapidly growing field [35]. This study expands on such studies, but it is important to note that the elastic dielectric (membrane bilayer) was not placed in air, but in a liquid electrolyte. This significantly changes the balance of the 'external' forces that act to bend the charged membrane. The interaction of fixed charges on the interior surface of the membrane with the electric field results in Coulomb force, which is a 'surface force', because the fixed charges are present only on the surface (internal) of the membrane. In present simulations it is the most prominent force acting on the membrane. It is markedly curtailed by the accumulations of counter-ions (and depletions of co-ions) in the Debye layer near the membrane. In the absence of the resting potential (i.e. the potential difference between the intracellular and extracellular compartments), this force always acts to bend the membrane toward the surface where the fixed charges are located, regardless of the sign of the charges. The Coulomb force vs. fixed charge density relationship is quadratic and sign independent, because the Coulomb force is a product of the fixed charge and the electric field (which is linearly related to the density of fixed charges). The resting potential also affects the electric field and thus the Coulomb force at the membrane surface, but only moderately, but if its contribution is strong enough and in opposite direction to that of the fixed charges, the membrane will bend away from the surface with the fixed charges. In great majority of cases however the Coulomb force, being much greater bends the membrane toward the surface with fixed charges.

Since an important contribution of this work is the inclusion of the dielectric force in the analysis of bending of the charged bilayer in the liquid electrolyte, it is necessary to provide a brief comment of what dielectric forces are and how they are evaluated. The polarization of molecular dipoles induced by the electric field creates the forces in the dielectric by acting on these dipoles [31], and produces a stress field known as the Maxwell stress [32,33]. The dielectric force acting on a membrane can be calculated, if the permittivities of the membrane and solution, as well as Maxwell stress tensor are known. One needs only to calculate the Maxwell stress tensor at the interface between the membrane and the solution, and not at any point in the membrane or in the solution. The dielectric force can thus simply be evaluated as a surface force by integration of the Maxwell stress over the surface of the membrane [33,34]. Counter-intuitively the dielectric force is completely independent of what the Maxwell stress tensor is within the membrane, or in the solution. However, unlike the Coulomb force that acts only on the upper membrane surface, i.e. where the fixed charges are located, the dielectric force acts on both upper and lower surface. Nevertheless, its values on the upper surface are much greater than at the lower surface, because the electric field at the higher surface is much greater.

Since the Maxwell stress is proportional to the dielectric constant (see Methods section), and given the differences in the permittivity (the permittivity of the membrane is 2 and that of the solution is 80), the dielectric force always acts from the solution toward the membrane. This is in contrast to the elastic dielectrics placed in the air [35,34]. Consequently the dielectric force at the upper surface always acts downwards, i.e. to curtail the Coulomb force, which as already mentioned almost always acts upwards. Given that the

relationship between the dielectric force and the electric field is quadratic (the Maxwell stress depends upon the electric field to the second order; see Methods section) the dielectric force vs. fixed charge density relationship is also quadratic, because the electric field is linearly related to the fixed charge density. As this study shows the dielectric force is not negligible, compared to the Coulomb force. Nevertheless, note that our finite element evaluations of the electrostatics are confined to the first-order dielectrics, and do not include higher order dielectric forces or generally of dielectric contributions [43]. We consider it unlikely that the higher order dielectric forces will contribute significantly to the electrostatics of the problem or to the dielectric force.

4.4. Spontaneous curvature

It is generally accepted that the curvature of biological membranes is influenced by the proteins able to bend membranes by scaffolding curvature and/or by hydrophobic insertion of "wedges" [19,6,7,20,13,5]. Such areas of high curvature are also generally believed to be important for the action of many biological processes. Recent studies have shown that some proteins such as Bin/Amphiphysin/Rvs domains [9], and amphipathic α-helices [12,11] upconcentrate on areas of high membrane curvature. In this study we show how a bilayer in a liquid electrolyte undergoes mechanical deformation in the presence of an electric field generated either by the 'resting potential' and/or by the presence of fixed charges on its surface. We quantified the membrane deformation of such an electro-active bilayer by simply determining how much the midpoint at the upper surface of the membrane becomes displaced vertically (in *z*-direction). This displacement increases in a supra-linear manner as fixed charge density rises, not surprisingly given that the forces driving the deformation – the Coulomb force and the dielectric force – are quadratic (i.e. supra-linear). The shape of the deformed membrane, though not perfectly circular can be well fitted by a circle, and can thus be characterized by a single number — a spontaneous curvature or a spontaneous radius. Both depend strongly and non-linearly on the density of fixed charges. At high density of fixed charges the spontaneous radius is approximately 50 nm. The fixed charges can thus make an important contribution to the curvature of membranes, and if the charge density is high this contribution may be important even at the curvature levels observed at organelles (granules, endoplasmic reticulum, etc.).

As shown in Results section neither the magnitude of the z-component of the electric field on the upper membrane surface nor membrane displacement (or membrane curvature) become much greater if the permittivity of the head sections of the membrane is four times higher (8 instead of 2). This may appear puzzling. According to Coulomb's law for interacting point charges in an infinite space the electric field at any point in space due to a single, discrete charge located at another point in space will decrease to 1/4 of its original value if permittivity of the medium increases by 4 times. The membrane however is finite and is immersed in liquid electrolyte, whose permittivity is much higher than that of membrane, and it effectively clamps the potential and the electric field, not only in the solution, but also in the membrane. The screening charges in the electrolyte provide an additional clamp. The electric field on the upper membrane surface and membrane displacement become more sensitive to the permittivity changes of the membrane, if the ion concentrations are reduced and screening charges are diminished and become more dispersed (not shown).

The spontaneous radius is in fact likely to be smaller (and the curvature greater) than these simulations show, because greater membrane tension will favor recruitment of membrane to the surface ('membrane tension hypothesis'; [44]). According to this hypothesis high tensions favor recruitment of membrane to the surface, whereas low tensions favor retrieval. Biological membranes expand elastically by up to 3% before rupture [45]. Beyond this limit, membrane area has to increase to avoid lysis. Indeed, as membrane capacitance measurements show during swelling, membrane is added from internal stores, whereas during shrinking, excess membrane is reinternalized [46] and membrane invaginates as vacuole-like dilations [47,48].

Finally, it is interesting to speculate about the potential advantages of having not just one, but several mechanisms involved in regulating membrane curvature. Various mechanisms may differ in speed. Some may have slower onset, but be of more permanent duration, whereas others may be faster, but also more transient. Insertion of proteins in the membrane is a slower, though more permanent process than changing for example fixed charges on the membrane surface by varying pH. Having not just one, but several tools in the toolkit enables one to respond better to changing needs and situations and provides also for more efficient cooperation. It is difficult to demonstrate when different membrane re-shaping mechanisms became prominent evolutionarily, but the electrostatic-bending was probably one of the first to have been used, as it can be implemented using a simple and rapid physical mechanism, such as pH-induced change of the fixed charge density on the membrane surface.

4.5. Dynamics of membrane deformation and elastic energy vs. displacement relationship

This study provides an assessment of how much the membrane bends given the presence of fixed charges on the membrane surface (and thus given the electrostatic and electrokinetic forces they induce), and the elastic properties of the membrane. It also shows that the bending occurs quickly, with a time constant of ~1 ms. This is interesting, because many signaling and membrane processes influenced by membrane bending [9–13,5] occur on such a time scale. Membrane bending can thus be seen as a memory element on a comparatively short time scale. The speed of bending is determined by the membrane elastic properties, because the electric force (the sum of Coulomb and dielectric forces) remains constant during bending. Note however that this study does not take into account the fluidic contribution to membrane bending or to its dynamics. This will be part of a separate study.

Acknowledgements

This work was supported by the grant from the National Sciences and Engineering Research Council of Canada and Canadian Heart and Stroke Foundation to M.I.G.

Appendix A

The bilayer model used in this study assumes that the two layers are not allowed to slide against each other; they are "glued" together [4].

Structural analysis

The structural analysis is implemented using the equilibrium equations, that balance the forces acting on the membranes, and the shape and displacement are determined using a method, which minimizes the energy functional of such a structure [39,40].

Equilibrium equations

The equilibrium equations expressed in terms of stresses and in 3D Cartesian coordinate system are:

$$-\frac{\partial \sigma_x}{\partial x}-\frac{\partial \tau_{xy}}{\partial y}-\frac{\partial \tau_{xz}}{\partial z}=F_x \tag{1a}$$

$$-\frac{\partial \tau_{xy}}{\partial x}-\frac{\partial \sigma_y}{\partial y}-\frac{\partial \tau_{yz}}{\partial z}=F_y \tag{1b}$$

$$-\frac{\partial \tau_{xz}}{\partial x}-\frac{\partial \tau_{yz}}{\partial y}-\frac{\partial \sigma_z}{\partial z}=F_z \tag{1c}$$

where **F** stands for the body forces. σ_x, σ_y, and σ_z are the three normal stresses and τ_{xy}, τ_{yz} and τ_{xz}, are the shear stresses, that together make up the symmetric stress tensor ($\boldsymbol{\sigma}$) for small deformations:

$$\sigma=\begin{bmatrix}\sigma_x & \tau_{xy} & \tau_{xz}\\ \tau_{yx} & \sigma_y & \tau_{yz}\\ \tau_{zx} & \tau_{zy} & \sigma_z\end{bmatrix}. \text{ Note also that : } \tau_{xy}=\tau_{yx}\ \ \tau_{xz}=\tau_{zx}\ \ \tau_{yz}=\tau_{zy}. \tag{2}$$

Eq. (3) expresses Eqs. (1a), (1b) and (1c) in the matrix notation:

$$-\nabla.\sigma=\mathbf{F} \tag{3}$$

Since the structural deformation of the lipid membrane is analyzed in terms of displacements, we need to establish the stress–strain and strain–displacement relationships and substitute them in Eq. (3).

Strain–displacement relationship

The strain can consist of initial (ε_0), thermal (ε_{th}) and elastic (ε_{el}) strain, but we neglect the first two terms and only consider the elastic strain ε_{el}. If *u*, *v*, and *w* are three elements of the displacement at a given point in the 3D coordinate system, assuming that the displacements are small, the relationship between the strains and displacements and their derivatives are as follows:

$$\varepsilon_x=\frac{\partial u}{\partial x}\quad \varepsilon_{xy}=\frac{\gamma_{xy}}{2}=\frac{1}{2}\left(\frac{\partial u}{\partial y}+\frac{\partial v}{\partial x}\right) \tag{4a}$$

$$\varepsilon_y=\frac{\partial v}{\partial y}\quad \varepsilon_{yz}=\frac{\gamma_{yz}}{2}=\frac{1}{2}\left(\frac{\partial v}{\partial z}+\frac{\partial w}{\partial y}\right) \tag{4b}$$

$$\varepsilon_z=\frac{\partial w}{\partial z}\quad \varepsilon_{xz}=\frac{\gamma_{xz}}{2}=\frac{1}{2}\left(\frac{\partial u}{\partial z}+\frac{\partial w}{\partial x}\right) \tag{4c}$$

where ε_x, ε_y, and ε_z are the normal strain elements, whereas ε_{xy}, ε_{yz}, and ε_{xz} are the shear strain components. The symmetric strain tensor is then:

$$\varepsilon=\begin{bmatrix}\varepsilon_x & \varepsilon_{xy} & \varepsilon_{xz}\\ \varepsilon_{xy} & \varepsilon_y & \varepsilon_{yz}\\ \varepsilon_{xz} & \varepsilon_{yz} & \varepsilon_z\end{bmatrix}. \tag{5}$$

Large displacements

If the system undergoes large deformations Eqs. (4a), (4b), and (4c) are no longer valid, and the strain–displacement relationship becomes:

$$\varepsilon_{ij}=\frac{1}{2}\left(\frac{\partial u_i}{\partial x_j}+\frac{\partial u_j}{\partial x_i}+\frac{\partial u_k}{\partial x_i}.\frac{\partial u_k}{\partial x_j}\right) \tag{6}$$

where *i*, *j*, *k* = 1, 2, 3 in the 3D coordinate system.

Energy minimization

In order to simulate the membrane deformation we implemented the energy minimization by using the principle of virtual work, which states that the sum of virtual work due to internal strains equals the work due to external forces. In such a case the following equation holds:

$$\delta W=0 \tag{7}$$

where *W* is the total stored energy from external and internal forces and strains as defined below:

$$\mathrm{W}=\int_V\left(\frac{1}{2}\left(-\varepsilon_x\sigma_x-\varepsilon_y\sigma_y-\varepsilon_z\sigma_z-2\varepsilon_{xy}\tau_{xy}-2\varepsilon_{yz}\tau_{yz}-2\varepsilon_{xz}\tau_{xz}\right)+\mathbf{u}^t\mathbf{F}_V\right)dv \tag{8}$$
$$+\int_S\mathbf{u}^t\mathbf{F}_S ds+\int_L\mathbf{u}^t\mathbf{F}_L dl+\sum\nolimits_P\mathbf{U}^t\mathbf{F}_P$$

V, *S*, *L*, and *P* stand for the body, surface, edge, and point in the material, respectively, whereas **U** and **u** are displacements of a given point in material.

Isotropic stress–strain relationship

We first consider the lipid membrane as a linear elastic material with a stress–strain relationship, or the constitutive equation, as:

$$\sigma=D\varepsilon_{\mathbf{el}}+\sigma_0=D\varepsilon. \tag{9}$$

We assume that the initial stress $\boldsymbol{\sigma_0}$ is zero. If the stress and strain are shown as column vectors:

$$\sigma=\begin{bmatrix}\sigma_x\\ \sigma_y\\ \sigma_z\\ \tau_{xy}\\ \tau_{yz}\\ \tau_{xz}\end{bmatrix}\quad \varepsilon=\begin{bmatrix}\varepsilon_x\\ \varepsilon_y\\ \varepsilon_z\\ \gamma_{xy}\\ \gamma_{yz}\\ \gamma_{xz}\end{bmatrix} \tag{10}$$

the elasticity matrix *D* is:

$$D=\frac{E}{(1+\nu)(1-2\nu)}\begin{bmatrix}1-\nu & \nu & \nu & 0 & 0 & 0\\ \nu & 1-\nu & \nu & 0 & 0 & 0\\ \nu & \nu & 1-\nu & 0 & 0 & 0\\ 0 & 0 & 0 & \frac{1-2\nu}{2} & 0 & 0\\ 0 & 0 & 0 & 0 & \frac{1-2\nu}{2} & 0\\ 0 & 0 & 0 & 0 & 0 & \frac{1-2\nu}{2}\end{bmatrix} \tag{11}$$

where *E* is Young's modulus and ν is Poisson's ratio. When an object is stretched the Poisson's ratio gives the ratio of the contraction (perpendicular to the applied load), to the extension in the direction of the applied load.

Anisotropic stress–strain relationship and equilibrium equation

If the material is anisotropic (we assume that the lateral fluidity of the membrane $\tau_{xy}=0$), the equilibrium equations have to be provided explicitly. They are given as follows:

$$\sigma_x=\sigma_y=\lambda_{xxxx}\left(\varepsilon_x+\varepsilon_y\right)+\lambda_{xxzz}\varepsilon_z \tag{12a}$$

$$\sigma_z=\lambda_{xxzz}\left(\varepsilon_x+\varepsilon_y\right)+\lambda_{zzzz}\varepsilon_z \tag{12b}$$

$$\tau_{xz}=\lambda_{xzxz}\gamma_{xz} \tag{12c}$$

$$\tau_{yz}=\lambda_{xzxz}\gamma_{yz}. \tag{12d}$$

Substituting Eqs. (4a), (4b), and (4c) into Eqs. (12a), (12b), (12c), and (12d) and subsequently into Eq. (1), the anisotropic equilibrium

equation in the 3D coordinate system reads:

$$\lambda_{xxxx}\left(\frac{\partial^2 u}{\partial x^2}+\frac{\partial^2 v}{\partial x\partial y}\right)+\lambda_{xzxz}\frac{\partial^2 u}{\partial z^2}+(\lambda_{xxzz}+\lambda_{xzxz})\frac{\partial^2 w}{\partial x\partial z}=-F_x \tag{13a}$$

$$\lambda_{xxxx}\left(\frac{\partial^2 v}{\partial y^2}+\frac{\partial^2 u}{\partial x\partial y}\right)+\lambda_{xzxz}\frac{\partial^2 v}{\partial z^2}+(\lambda_{xxzz}+\lambda_{xzxz})\frac{\partial^2 w}{\partial y\partial z}=-F_y \tag{13b}$$

$$\lambda_{xzxz}\left(\frac{\partial^2 w}{\partial x^2}+\frac{\partial^2 w}{\partial y^2}\right)+\lambda_{zzzz}\frac{\partial^2 w}{\partial z^2}+(\lambda_{xxzz}+\lambda_{xzxz})\left(\frac{\partial^2 u}{\partial x\partial z}+\frac{\partial^2 v}{\partial y\partial z}\right)=-F_z. \tag{13c}$$

In the case of the 2D model in the *x*-*z* plane, Eqs. (13a), (13b), and (13c) is simplified into the following set of equations:

$$\lambda_{xxxx}\frac{\partial^2 u}{\partial x^2}+\lambda_{xzxz}\frac{\partial^2 u}{\partial z^2}+(\lambda_{xxzz}+\lambda_{xzxz})\frac{\partial^2 w}{\partial x\partial z}=-F_x \tag{14a}$$

$$\lambda_{xzxz}\frac{\partial^2 w}{\partial x^2}+\lambda_{zzzz}\frac{\partial^2 w}{\partial z^2}+(\lambda_{xxzz}+\lambda_{xzxz})\frac{\partial^2 u}{\partial x\partial z}=-F_z \tag{14b}$$

λ_{xxxx} and λ_{zzzz} are Young's moduli of volume stretching-compression in the lateral and normal direction respectively, and λ_{xxzz} is the Young's modulus of coupling between lateral and normal deformation. Finally, λ_{xzxz} is Young's modulus of transverse shear deformation, which is vanishing in the case of coupled monolayers [4]. All values are given in Table 2.

The elasticity matrix of the 3D anisotropic model is then:

$$D=\begin{bmatrix}\lambda_{xxxx} & \lambda_{xxxx} & \lambda_{xxzz} & 0 & 0 & 0\\ \lambda_{xxxx} & \lambda_{xxxx} & \lambda_{xxzz} & 0 & 0 & 0\\ \lambda_{xxzz} & \lambda_{xxzz} & \lambda_{zzzz} & 0 & 0 & 0\\ 0 & 0 & 0 & 0 & 0 & 0\\ 0 & 0 & 0 & 0 & \lambda_{xzxz} & 0\\ 0 & 0 & 0 & 0 & 0 & \lambda_{xzxz}\end{bmatrix} \tag{15}$$

The elasticity matrix of the 2D anisotropic model then becomes:

$$D=\begin{bmatrix}\lambda_{xxxx} & \lambda_{xxxx} & \lambda_{xxzz}\\ \lambda_{xxxx} & \lambda_{xxxx} & \lambda_{xxzz}\\ \lambda_{xxzz} & \lambda_{xxzz} & \lambda_{zzzz}\end{bmatrix}. \tag{16}$$

Elastic energy density

According to the standard theory of elasticity [39,40] the elastic energy density (J/m^3) of an anisotropic 3D structure is described as follows:

$$f=\sigma^0_{ij}\varepsilon_{ij}+\frac{1}{2}\lambda_{ijlm}\varepsilon_{ij}\varepsilon_{lm}. \tag{17}$$

We denote the tensor of the elastic moduli of the lipid monolayer as λ_{ijlm}, whereas ε_{ij} represents the strain tensor defined above, and if the initial stress σ^0_{ij} is taken to be zero the above equation becomes:

$$f=\frac{1}{2}\sigma.\varepsilon. \tag{18}$$

Substituting the elements of the **σ** and **ε** matrices into Eq. (17) finally yields the equation for the elastic energy density:

$$f=\frac{1}{2}\left(\varepsilon_x\sigma_x+\varepsilon_y\sigma_y+\varepsilon_z\sigma_z+2\varepsilon_{xy}\tau_{xy}+2\varepsilon_{yz}\tau_{yz}+2\varepsilon_{xz}\tau_{xz}\right). \tag{19}$$

Surface traction

The *i*-th component of the surface traction (force/area) in the 3D case is given by the following equation:

$$T_i=\sigma_{ij}n_j\Rightarrow\begin{bmatrix}T_x\\ T_y\\ T_z\end{bmatrix}=\begin{bmatrix}\sigma_x & \tau_{xy} & \tau_{xz}\\ \tau_{xy} & \sigma_y & \tau_{yz}\\ \tau_{xz} & \tau_{yz} & \sigma_z\end{bmatrix}.\begin{bmatrix}n_x\\ n_y\\ n_z\end{bmatrix}. \tag{20}$$

References

[1] W. Helfrich, Elastic properties of lipid bilayers: theory and possible experiments, Z. Naturforsch. C 28 (1973) 693–703.
[2] E.A. Evans, R.M. Hochmuth, Mechanochemical properties of membranes, Curr. Top. Membr. Transp. 10 (1978) 1–62.
[3] E.A. Evans, A. Young, Hidden dynamics in rapid changes in bilayer shape, Chem. Phys. Lipids 73 (1994) 39–56.
[4] F. Campello, H.T. McMahon, M.M. Kozlov, The hydrophobic insertion mechanism of membrane curvature generation by proteins, Biophys. J. 95 (2008) 2325–2339.
[5] N.S. Hatzakis, V.K. Bhatia, J. Larsen, K.L. Madsen, P.Y. Bolinge, A.H. Kunding, J. Castillo, U. Gether, P. Hedegård, D. Stamou, How curved membranes recruit amphipathic helices and protein anchoring motifs, Nat. Chem. Biol. 5 (2009) 835–841.
[6] H.T. McMahon, J.L. Gallop, Membrane curvature and mechanisms of dynamic cell membrane remodeling, Nature 438 (2005) 590–596.
[7] J. Zimmerberg, M.M. Kozlov, How proteins produce cellular membrane curvature, Nat. Rev. Mol. Cell Biol. 7 (2006) 9–19.
[8] M. Tajparast, M.I. Glavinović, Extrusion of transmitter, water and ions generates forces to close fusion pore, Biophys. Biochem. Acta 1788 (2009) 993–1008.
[9] B.J. Peter, H.M. Kent, I.G. Mills, Y. Vallis, P.J.G. Butler, P.R. Evans, H.T. McMahon, BAR domains as sensors of membrane curvature: the amphiphysin BAR structure, Science 303 (2004) 495–499.
[10] A. Roux, D. Cuvelier, P. Nassoy, J. Prost, P. Bassereau, B. Goud, Role of curvature and phase transition in lipid sorting and fission of membrane tubules, EMBO J. 24 (2005) 1537–1545.
[11] R.B. Cornell, S.G. Taneva, Amphipathic helices as mediators of the membrane interaction of amphitropic proteins, and as modulators of bilayer physical properties, Curr. Protein Pept. Sci. 7 (2006) 539–552.
[12] G. Drin, J.F. Casella, R. Gautier, T. Boehmer, T.U. Schwartz, B. Antonny, A general amphipathic alpha-helical motif for sensing membrane curvature, Nat. Struct. Mol. Biol. 14 (2007) 138–146.
[13] R. Parthasarathy, J.T. Groves, Curvature and spatial organization in biological membranes, Soft Matter 3 (2007) 24–33.
[14] V.A. Frolov, J. Zimmerberg, Shaping biological matter, Nat. New Biol. 8 (2009) 173–174.
[15] J. Gruenberg, F.R. Maxfield, Membrane transport in the endocytic pathway, Curr. Opin. Cell Biol. 7 (1995) 552–563.
[16] H. Lodish, D. Baltimore, A. Berk, S.L. Zipurski, P. Matsudaira, J. Darnell, Molecular Cell Biology, Scientific American Books Inc, New York, USA, 1995.
[17] J.E. Rothman, Mechanisms of intracellular protein transport, Nature 372 (1994) 55–63.
[18] R. Schekman, L. Orci, Coat proteins and vesicle budding, Science 271 (1996) 1526–1533.
[19] K. Farsad, P. De Camilli, Mechanisms of membrane deformation, Curr. Opin. Cell Biol. 15 (2003) 372–381.
[20] G.K. Voeltz, W.A. Prinz, Sheets, ribbons and tubules — how organelles get their shape, Nat. Rev. Mol. Cell Biol. 8 (2007) 258–264.
[21] M. Tajparast, M.I. Glavinović, Forces and stresses acting on fusion pore membrane during secretion, Biophys. Biochem. Acta 1788 (2009) 1009–1023.
[22] T. Kirchhausen, Three ways to make a vesicle, Nat. Rev. Mol. Cell Biol. 1 (2000) 187–198.
[23] B. Antonny, Membrane deformation by protein coats, Curr. Opin. Cell Biol. 18 (2006) 386–394.
[24] Y. Shibata, J. Hu, M.M. Kozlov, T.A. Rapoport, Mechanisms shaping the membranes of cellular organelles, Annu. Rev. Cell Dev. Biol. 25 (2009) 329–354.
[25] M. Winterhalter, W. Helfrich, Effect of surface charge on the curvature elasticity of membranes, J. Phys. Chem. 92 (1988) 6865–6867.
[26] D.J. Mitchell, B.W. Ninham, Curvature elasticity of charged membranes, Langmuir 5 (1989) 1121–1123.
[27] B. Duplantier, R.E. Goldstein, V. Romero-Rochin, A.I. Pesci, Geometrical and topological aspects of electric double layers near curved surfaces, Phys. Rev. Lett. 65 (1990) 508–511.
[28] M. Winterhalter, W. Helfrich, Bending elasticity of electrically charged bilayers: coupled monolayers, neutral surfaces, and balancing stresses, J. Phys. Chem. 96 (1992) 327–330.
[29] T. Chou, M.V. Jaric, E.D. Siggia, Electrostatics of lipid bilayer bending, Biophys. J. 72 (1997) 2042–2055.
[30] P. De Camilli, S.D. Emr, P.S. McPherson, P. Novick, Phosphoinositides as regulators in membrane traffic, Science 271 (1996) 1533–1539.
[31] H.A. Pohl, Some effects of nonuniform fields on dielectrics, J. Appl. Phys. 29 (1958) 1182–1188.
[32] K.R. Foster, A.E. Sowers, Dielectrophoretic forces and potentials induced on pairs of cells in an electric field, Biophys. J. 69 (1995) 777–784.

[33] K.H. Kang, D. Li, Dielectric force and relative motion between two spherical particles in electrophoresis, Langmuir 22 (2006) 1602–1608.
[34] G. Kofod, The static actuation of dielectric elastomer actuators: how does pre-stretch improve actuation? J. Phys. D: Appl. Phys. 41 (2008) 1–11.
[35] M. Wissler, E. Mazza, Mechanical behavior of an acrylic elastomer used in dielectric elastomer actuators, Sens. Actuators A 134 (2007) 494–504.
[36] S.G.A. McLaughlin, G. Szabo, G. Eisenman, Divalent ions and the surface potential of charged phospholipid membranes, J. Gen. Physiol. 58 (1971) 667–687.
[37] B. Hille, A.M. Woodhull, B.I. Shapiro, Negative surface charge near sodium channels of nerve: divalent ions, monovalent ions, and pH, Philos. Trans. R. Soc. (Lond.) B Biol. Sci. 270 (1975) 301–318.
[38] R.E. Pelrine, R.D. Kornbluh, J.P. Joseph, Electrostriction of polymer dielectrics with compliant electrodes as a means of actuation, Sens. Actuators A 64 (1998) 77–85.
[39] A.I. Lurie, Theory of Elasticity, Springer, 1999.
[40] L.D. Landau, E.M. Lifshitz, Theory of Elasticity, Pergamon, Oxford, UK, 1986.
[41] J.D. Jackson, Classical Electrodynamics, Wiley, New York, 1999.
[42] G. Karniadakis, A. Beskok, N. Aluru, Microflows and Nanoflows. Fundamentals and Simulation, Springer, 2005.
[43] C.H. Kua, Y.C. Lam, C. Yang, K. Youcef-Toumi, I. Rodriguez, Modeling of dielectrophoretic force for moving dielectrophoresis electrodes, J. Electrostat. 66 (2008) 514–525.
[44] J. Dai, M.P. Sheetz, X. Wan, C.E. Morris, Membrane tension in swelling and shrinking molluscan neurons, J. Neurosci. 18 (1998) 6681–6692.
[45] J.A. Nichol, O.F. Hutter, Tensile strength and dilatational elasticity of giant sarcolemmal vesicles shed from rabbit muscle, J. Physiol. (Lond) 493 (1996) 187–198.
[46] V.L. Sukhorukov, W.M. Arnold, U. Zimmermann, Hypotonically induced changes in the plasma membrane of cultured mammalian cells, J. Membr. Biol. 132 (1993) 27–40.
[47] S.A. Krolenko, W.B. Amos, J.A. Lucy, Reversible vacuolation of the transverse tubules of frog skeletal muscle: a confocal fluorescence microscope study, J. Muscle Res. Cell Motil. 16 (1995) 401–411.
[48] C. Reuzeau, L.R. Mills, J.A. Harris, C.E. Morris, Discrete and reversible vacuole-like dilations induced by osmo-mechanical perturbations of neurons, J. Membr. Biol. 145 (1995) 33–47.